Advanced silicon processing for active planar photonic devices

Michael Shearn, Kenneth Diest, Xiankai Sun, Avi Zadok, Harry Atwater, Amnon Yariv, and Axel Scherer

Citation: Journal of Vacuum Science & Technology B **27**, 3180 (2009); doi: 10.1116/1.3256649
View online: http://dx.doi.org/10.1116/1.3256649
View Table of Contents: http://scitation.aip.org/content/avs/journal/jvstb/27/6?ver=pdfcov
Published by the AVS: Science & Technology of Materials, Interfaces, and Processing

Articles you may be interested in

Loss management using parity-selective barriers for single-mode, single-cell photonic crystal resonators
Appl. Phys. Lett. **88**, 161119 (2006); 10.1063/1.2193651

Reactive ion etching induced damage evaluation for optoelectronic device fabrication
J. Vac. Sci. Technol. B **24**, 756 (2006); 10.1116/1.2181576

High power, single-mode operation from photonic-lattice semiconductor lasers with controllable lateral resonance
Appl. Phys. Lett. **88**, 091112 (2006); 10.1063/1.2180443

Low-loss photonic crystal defect waveguides in InP
Appl. Phys. Lett. **84**, 3588 (2004); 10.1063/1.1737487

Channel optical waveguides formed by deuterium passivation in GaAs and InP
J. Appl. Phys. **82**, 3205 (1997); 10.1063/1.365626

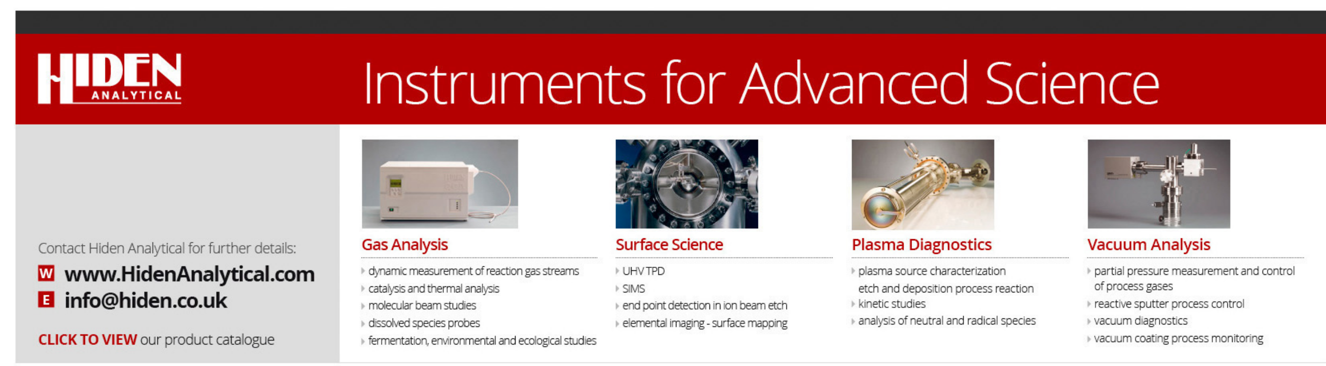

Redistribution subject to AVS license or copyright; see http://scitation.aip.org/termsconditions. Download to IP: 131.215.238.188 On: Sat, 20 Sep 2014 20:40:37

Advanced silicon processing for active planar photonic devices

Michael Shearn,[a] Kenneth Diest, Xiankai Sun, Avi Zadok, Harry Atwater, Amnon Yariv, and Axel Scherer
Thomas J. Watson Laboratory, California Institute of Technology, 1200 E. California Blvd., Pasadena, California 91125

(Received 8 July 2009; accepted 5 October 2009; published 7 December 2009)

Using high quality, anisotropically etched Si waveguides bonded to InGaAsP, the authors demonstrate a hybrid laser, whose optical profile overlaps both Si and III-V regions. Continuous wave laser operation was obtained up to 45 °C, with single facet power as high as 12.7 mW at 15 °C. Planar Si optical resonators with $Q=4.8\times10^6$ are also demonstrated. By using a SF_6/C_4F_8 reactive ion etch, followed by H_2SO_4/HF surface treatment and oxygen plasma oxide, the optical losses due to the waveguide and the bonding interface are minimized. Changes of optical confinement in the silicon are observed due to waveguide width variation. © *2009 American Vacuum Society.*
[DOI: 10.1116/1.3256649]

I. INTRODUCTION

Integrating silicon electronics with other materials systems is an important way to extend the capabilities of the microelectronics platform. Hybrid systems enable applications that were previously impossible or ineffective in silicon, such as lasers[1] and biosensing.[2] Hybrid optical systems are of particular interest, as they use silicon's capability for low loss passive waveguides[3] but use other materials to avoid functionality limitations from silicon's indirect bandgap. However, direct integration through epitaxy of these systems is problematic due to differences in the lattice constant and thermal expansion coefficients.[4] Recently, wafer-bonded III-V materials on Si waveguides have produced lasers[1,5] and modulators.[6] The bonded structure is designed to support a joint optical mode, whose profile overlaps both materials. This architecture is a promising step toward monolithic integration of electronics with optics.

In this article, we demonstrate operation of a hybrid Si/InGaAsP Fabry–Pérot laser and describe the processing steps and optimization in its production. Si waveguide quality is maximized using a low damage, high fidelity reactive ion etch, and subsequent surface treatment, characterized by Si ring resonator measurements. Low temperature, plasma-assisted wafer bonding[7] is then used to integrate the two material systems. Finally, optical and electrical measurements are made to characterize the hybrid laser.

II. FABRICATION METHODS

A. Pattern definition and plasma etching

Waveguide patterns were defined on silicon-on-insulator (SOI) wafers with a Si layer thickness from 220 to 900 nm on top of a 2 μm SiO_2 buried oxide layer using electron beam lithography. Zeon ZEP520A was spun as 5000 rpm and baked at 180 °C for 20 min before exposure with a 100 keV electron beam. After development, patterns were placed in an oven at 150 °C for 5 min to cause the resist to reflow, reducing pattern roughness.

The waveguide patterns were transferred using an anisotropic dry etch in an inductively coupled plasma reactive ion etcher (Oxford Instruments PlasmaLab System 100 ICP-RIE 380), with a typical etch profile seen in Fig. 1. We utilized a mixed mode plasma etch using SF_6 (an etch gas) and C_4F_8 (a polymer source gas), with process conditions as described in other publications.[8] In contrast to more traditional chopped processes such as the Bosch etch,[9] simultaneous etching and sidewall passivation offers improved sidewall smoothness and reasonable etch rates at room temperature.[10] Also important is the low forward rf power utilized by this etch, which reduces roughness from mask erosion. The etch depth varied in order to leave varying heights of Si remaining.

B. Wafer bonding, mesa definition, and metallization

After etching, the SOI wafer was cleaned by solvents and a 3:1 mixture of $H_2SO_4:H_2O_2$ (10 min at 170 °C), followed immediately by a HF dip to remove chemical oxide from the SOI wafer and native oxide from the III-V wafer, respectively. The reason for this cleaning step is twofold. First, it removes any remaining organics that would interfere with bonding. Second, it chemically prepares the surface for bonding by hydrogen terminating the surface, maximizing the effect of plasma activation.[7] Similar processing steps have also shown improvements in optical properties of waveguides through removal of absorbing surface states.[11]

After cleaning, the surfaces of the wafers were then activated through exposure to a low bias oxygen plasma and bonded together under a pressure of 0.1 MPa at 350 °C for 1 h. Following the bonding, the InP substrate was removed by HCl etching and mesa and contact structures were defined lithographically and etched. A mesa structure, centered above the Si waveguide, was formed in the InGaAsP layers using photolithography and a three-phase wet etch. The etching solutions were (i) 1:1:10 mixture of $H_2SO_4:H_2O_2:H_2O$

[a]Electronic mail: mshearn@caltech.edu

Redistribution subject to AVS license or copyright; see http://scitation.aip.org/termsconditions. Download to IP: 131.215.238.188 On: Sat, 20 Sep 2014 20:40:37

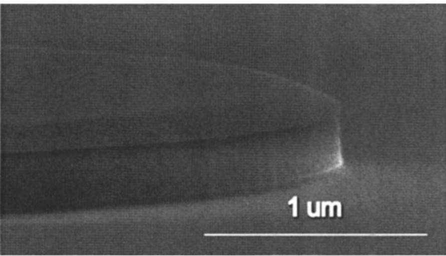

FIG. 1. Profile of a fully etched disk structure on a SOI wafer with resist. The slope of the resist is caused by reflow.

(*p*-InGaAs layer, 60 s), (ii) 2:1 mixture of HCl:H_2O (*p*-InP layer, 30 s), and (iii) 1:1:10 mixture of H_2SO_4:H_2O_2:H_2O (quaternary layers, 4 min). Contacts consisting of Cr/AuZn/Au for the *p*-side metallization (on top of mesa) and Cr/AuGe/Au for the *n*-side metallization (to side of mesa) were deposited by thermal evaporation. The current flow was laterally confined by means of proton implantation at an areal dose of 5×10^{14} cm^{-2} and an energy of 170 keV, resulting in high resistance except in a 5 μm channel. Finally, the Si substrate was thinned mechanically to increase thermal conductivity to the testing chuck, resulting in a structure, as shown in Fig. 2.

III. DEVICE MEASUREMENTS

A. Microring resonators

To determine the compatibility of the wafer bonding chemical treatments with low loss photonic structures, we fabricated bare silicon microrings using the same processing steps used for wafer-bonded samples. The devices were fabricated from a SOI wafer with a 220 nm thick Si device layer on a 2 μm SiO_2 buried oxide layer, and measured using evanescent coupling from a tapered fiber.[12] On these devices, a thin 30 nm thermal oxide was grown; this differs from wafer-bonded devices which we discovered only required an ultrathin oxide formed from O_2 plasma treatment.

The quality factor Q of the resonator was determined experimentally from the normalized fiber transmission spectrum under weak coupling to the ring. Due to poor phase matching between the fiber and microring modes, coupling is very low even when the fiber is nearly in contact with the

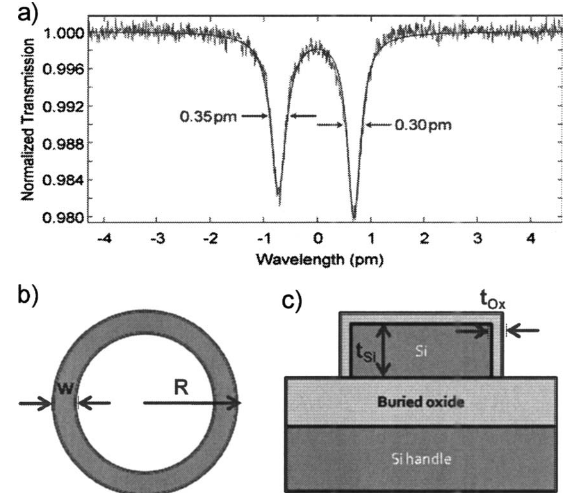

FIG. 3. Measurements and schematic of a high-Q microring resonator. (a) Taper transmission versus wavelength of a doublet mode for a microring with $R=40$ μm, $w=2$ μm $t_{Si}\approx200$ nm, $t_{ox}\approx30$ nm. (b) Top view of microring. (c) Cross-sectional view of microring.

ring. However, in this regime the measured Q is nearly the intrinsic Q. Figure 3 show results from a ring with $Q=4.1\times10^6$ and $Q=4.8\times10^6$ for the short and long wavelength modes, respectively. This corresponds with a loss of approximately 0.14 dB/cm. The two modes in the spectrum are a result of coupling due to scattering between the otherwise degenerate clockwise and counterclockwise circulating modes, and are only present because of the otherwise low loss of the waveguide structure.[13,14]

This initial result of a high quality planar structure, as opposed to freestanding geometries,[15] led us to pursue wafer-bonded structures that incorporate gain with the waveguide.

B. Hybrid lasers

We tested Fabry–Pérot hybrid lasers with lengths from 300 to 1500 μm. The Si waveguides were defined on a SOI wafer with 900 nm thick Si device layer on a 2 μm SiO_2 buried oxide layer. Results of a typical hybrid laser are shown in Fig. 4, which shows a device with a lasing threshold voltage V_{th} of 1.3 V and a threshold current density J_{th} of 1.25 kA/cm^2. The maximum power output from a single fa-

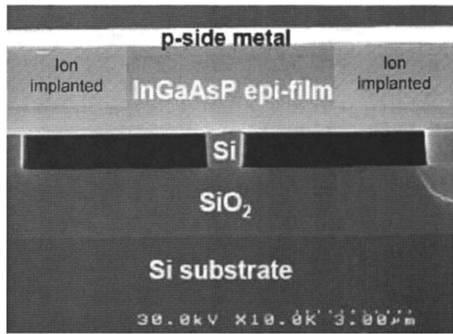

FIG. 2. Cross section of a typical bonded device. *N*-side contacts are to either side of the device (not pictured).

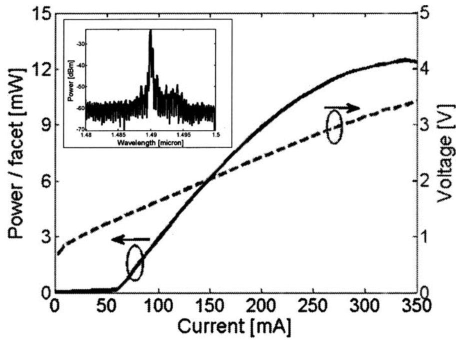

FIG. 4. *L-I-V* curve of a 960-μm-long laser operating in CW mode at 15 °C. (Inset) Laser spectrum.

Redistribution subject to AVS license or copyright; see http://scitation.aip.org/termsconditions. Download to IP: 131.215.238.188 On: Sat, 20 Sep 2014 20:40:37

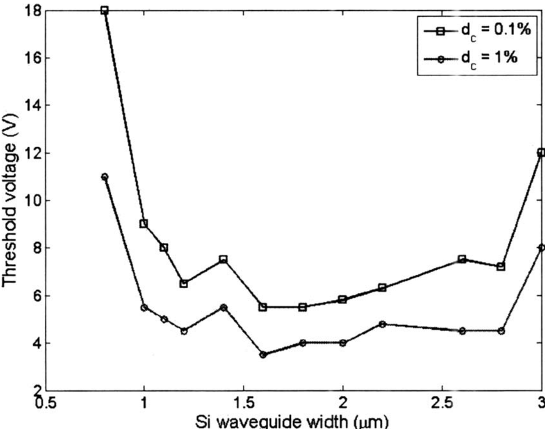

FIG. 5. Threshold voltage of hybrid lasers with various Si waveguide widths. Measurements were taken in pulsed mode at 15 °C, with d_c denoting the duty cycle of the applied voltage.

cet was 12.7 mW at 15 °C. The inset of Fig. 4 shows the laser spectrum with a central wavelength of 1490 nm.

On varying the Si waveguide width w, V_{th} was found to have a local minimum at $w \sim 1.5$ μm, with dependence shown in Fig. 5. This behavior can be understood qualitatively by considering the two limiting cases of waveguide width. As width decreases, less of the mode resides in the silicon, and thus experiences less feedback from the Si facets, which are of higher reflectivity than those in the III-V. On the other hand, as width increases, the mode is less confined to the quantum well region and thus requires a higher pump level to reach threshold. Further work on investigating this effect and optimizing our gain structure to utilize the relative strengths of these two regimes is underway.

IV. CONCLUSIONS

We have shown how care in silicon processing steps for hybrid systems can lead to good optical performance. Low loss Si waveguides can be fabricated using resist reflow, low-bias dry etching, and surface chemical treatments. Subsequent integration of these optical structures at low temperature is possible with plasma-assisted wafer bonding. By using the CMOS compatible processes described, we can integrate optics with electronics seamlessly without significantly altering the constraints on upstream processing steps on the silicon. Further improvement is possible with supermode engineering[16] or new materials systems, and will make this architecture even more attractive.

ACKNOWLEDGMENTS

This work was supported by Defense Advanced Research Projects Agency (DARPA) Contract No. N66001-07-1-2058 and HR0011-04-1-0054, the U.S. Air Force Office of Scientific Research (AFOSR) Grant No. FA9550-06-1-0480, and the Center for Science and Engineering of Materials, a National Science Foundation (NSF) Materials Research Science and Engineering Center at Caltech. The authors thank the Kavli Nanoscience Institute, Caltech, for supporting fabrication. M.S. thanks the NSF Graduate Research Fellowship program. A.Z. acknowledges postdoctoral fellowships from the Center for the Physics of Information, Caltech, and the Rothschild fellowship from Yad-Hanadiv Foundation, Israel.

[1] A. W. Fang, H. Park, O. Cohen, R. Jones, M. J. Paniccia, and J. E. Bowers, Opt. Express **14**, 9203 (2006).
[2] R. Pantoja, J. M. Nagarah, D. M. Starace N. A. Melosh, R. Blunck, F. Bezanilla, and J. R. Heath, Biosens. Bioelectron. **20**, 509 (2004).
[3] D. A. B. Miller, IEEE J. Sel. Top. Quantum Electron. **6**, 1312 (2000).
[4] H. Kroemer, T.-Y. Liu, and P. M. Petroff, J. Cryst. Growth **95**, 96 (1989).
[5] X. Sun, A. Zadok, M. J. Shearn K A. Diest, A. Ghaffari, H. A. Atwater, A. Scherer, and A. Yariv, Opt. Lett. **34**, 1345 (2009).
[6] H.-W. Chen, Y.-h. Kuo, and J. E. , Opt. Express **16**, 20571 (2008).
[7] D. Pasquariello and K. Hjort, IEEE J. Sel. Top. Quantum Electron. **8**, 118 (2002).
[8] M. D. Henry, S. Walavalkar, A. Homyk, and A. Scherer, Nanotechnology **20**, 255305 (2009).
[9] S. Rauf, W. J. Dauksher, S. B. Clemens, and K. H. Smith, J. Vac. Sci. Technol. A **20**, 1177 (2002).
[10] H. Jansen, M. de Boer, R. Legtenberg, and M. Elwenspoek, J. Micromech. Microeng. **5**, 115 (1995).
[11] M. Borselli, T. J. Johnson, and O. Painter, Appl. Phys. Lett. **88**, 131114 (2006).
[12] M. Borselli, K. Srinivasan, P. E. Barclay, and O. Painter, Appl. Phys. Lett. **85**, 3693 (2004).
[13] M. Borselli, T. Johnson, and O. Painter, Opt. Express **13**, 1515 (2005).
[14] M. L. Gorodetsky, A. D. Pryamikov, and V. S. Ilchenko, J. Opt. Soc. Am. B **17**, 1051 (2000).
[15] D. K. Armani, T. J. Kippenberg, S. M. Spillane, and K. J. Vahala, Nature **421**, 925 (2003); M. Cai, O. Painter, and K. J. Vahala, Phys. Rev. Lett. **85**, 74 (2000).
[16] X. Sun and A. Yariv, J. Opt. Soc. Am. B **25**, 923 (2008).

Redistribution subject to AVS license or copyright; see http://scitation.aip.org/termsconditions. Download to IP: 131.215.238.188 On: Sat, 20 Sep 2014 20:40:37